

Dynamics simulation of positioning and assembling multi-microparticles utilizing optoelectronic tweezers

Xiaolu Zhu · Zhifeng Yin · Zhonghua Ni

Received: 2 August 2011 / Accepted: 11 October 2011 / Published online: 8 November 2011
© Springer-Verlag 2011

Abstract Optoelectronic tweezer (OET) has become a powerful and versatile technique for manipulating microparticles and cells using real-time reconfigurable optical patterns. However, detailed research in the *dynamics* of particles in an OET device is still scarce, and the multiple-particle interactions still need further quantitative investigation. In this study, a dynamics simulation model coupling optically induced dielectrophoretic force, interaction forces between particles, and hydrodynamic and sedimentary forces is established and numerically solved by utilizing a finite element method and a dynamics simulation frame for multi-microparticles' positioning and assembling in a typical OET device. The spatial distributions of particles in the energized OET device before optically projecting are simulated first and the condition for particle chain formation is discussed. Then, the most representative ring-shaped optical pattern is applied, and the influences of optical-ring tweezer' dimensions of inner radius R_e and width d_e on positioning and assembling effect are dynamically simulated and discussed for 5- and 2- μm radius particles. The simulation results indicate the particles inside and outside optical ring both undergo negative DEP and are distributed centre-symmetrically under the action of ring virtual tweezers. Average distance between the particle and center of ring (ADPC) at equilibrium and the system equilibrium time characterizing particle positioning effect dramatically

increase for both 5- and 2- μm radius particles while R_e increases from 35 to 55 μm . Specially, the captured particles will pile up and immediately form a three-dimensional micropylamid structure when R_e approximately equals 25 μm for the 5- μm radius particle. Moreover, ADPC decreases very slowly for both two particle-sizes and the system equilibrium time of 2- μm radius particle vary more obviously than that of 5- μm radius particle with d_e increasing from 10 to 30 μm . And the system equilibrium time for 2- μm radius particle is always larger than that for 5- μm radius particle. The primary simulation results are in good agreement with experimental observations; hence this dynamics simulation model can truly predict the particle-moving trajectory and equilibrium positions in an OET device. Moreover, this dynamics simulation holds promise for designing and optimizing optical patterns for accuracy in assembling particles in order to form a specific microstructure.

Keywords Dynamics simulation · Optoelectronic tweezers · Microparticle assembly · Microfluidics

1 Introduction

Dielectrophoresis (DEP) is the motion of neutral polarizable particles polarized in non-uniform electric fields (Pohl 1978). The net electric force of the polarized particles in non-uniform electric field is dielectrophoresis force. As a kind of non-contact, non-destructive manipulation technology, DEP is good at efficient separation, transportation, focusing, filtering and detection of colloids and biological particles to ensure the high-quality analysis of chemical and biological samples (Green and Morgan 1997; Morgan et al. 2003; Aldaeus et al. 2005; Cheng et al. 2007). In

X. Zhu · Z. Yin · Z. Ni (✉)
School of Mechanical Engineering,
Southeast University, Nanjing 211189, China
e-mail: nzh2003@seu.edu.cn

X. Zhu · Z. Yin · Z. Ni
Jiangsu Key Laboratory for Design and Manufacture
of Micro-Nano Biomedical Instruments,
Southeast University, Nanjing 211189, China

order to manipulate particles, metallic microelectrodes are usually designed and fabricated. The electrode configurations are commonly fixed and cannot be reconfigured in real-time, which leads to high cost and complexity and possibly restricts the flexibility in microparticles' manipulation applications. In order to break through the bottleneck of physical electrode, Wu's group (Chiou et al. 2005) puts forward optically induced dielectrophoresis (ODEP) technology, which is also visually called optoelectronic tweezers (OET). Based on photoconductive materials, optical virtual electrodes are able to be created on photoconductive film; thus the non-uniform electric field is produced, and then microparticles can be manipulated by dielectrophoresis force in the OET device.

Many publications on ODEP technology focused on the experimental research, such as the interactive manipulation of blood cells by ODEP (Hwang et al. 2008a), manipulation of semiconducting and metallic nanowires (Jamshidi et al. 2008), continuous microparticle counting and sorting (Lin and Lee 2008), parallel single-cell light-induced electroporation (Valley et al. 2009), separating particles utilizing ODEP force difference (Lin et al. 2010) and manipulation and patterning of carbon nanotubes (Lee et al. 2010). Additionally, some published papers have contributed to the aspect of simulation research for the understanding and analysis of the physics implied in DEP or ODEP phenomena. Ohta (2008) and Jamshidi (2009) modeled and simulated the principle of OET with the finite element method (FEM) and analyzed the positioning and assembling of micro and nano particles with optically induced electrodes. Hwang et al. (2008b) carried out basic simulation on two particles' interactive forces under ODEP and simulated the trajectory of the two particles. Li et al. (2008) simulated the electric field of optical virtual electrodes and compared the efficiencies of manipulating single particles by using an optical electrode and a physical electrode. Valley et al. (2008) presented the finite element modeling of the electrokinetic effect and investigated the operational regimes in the OET device. However, the motion of a particle polarized by the optically induced non-uniform electric fields in OET device significantly influenced by the force action of all other particles around it within a certain space range and this multi-particle effect has not been quantitatively investigated as yet. Moreover, the dynamic simulation for OET manipulation of particles has not been quantitatively investigated in earlier literature, and the dynamic process of particle movement is crucially important for better understanding and controlling the dynamic assembly of particles using the optical-ring virtual tweezer.

The numerical simulation method used to simulate the motion, trajectory and dynamic properties of particles can be divided into many types according to the simulation

principle. As one of the most effective dynamic simulation methods, the molecular dynamics (MD) simulation method is able to analyze colloidal particles' motion, and the motion equation of each particle could be solved on a step-by-step basis. The MD simulation method does not require the solving of Navier–Stokes equations, which has also shown great advantages in micro- and nano-particle dielectrophoresis (Salonen et al. 2005; Lin et al. 2006; Ni et al. 2009). However, the computation amount of MD simulation for dielectrophoresis of colloids in a complex electric field is relatively huge and becomes a great challenge to the hardware performance. The MD program for simulating colloidal DEP is commonly based on the polarizable colloidal particle model consisting of a large macroion and small bound microions (Salonen et al. 2005), and have to conduct a numerical computation of approximate 2 million simulating steps for $\sim 2,000$ – $20,000$ particles and each step takes about 1–2 s for computation. Especially, the total computational time will be prolonged when the MD simulation needs to be repeated many times for diverse electrode geometries and dimensions in order to design, analyze, and optimize the DEP-based microfluidics system.

In order to reduce computation time and hardware cost, FEM and a dynamics simulation (DS) framework are jointly considered in this paper. Firstly, electric fields in three-dimensional (3D) computing domain of OET device are calculated by FEM. Secondly, motion equations of microparticles driven by multiple physical forces in OET device are solved by using the dynamics simulation frame, then the kinetics of particles are calculated and the whole system's properties can be investigated. FEM is more efficient and flexible than typical MD methodology on calculation of complex or irregular geometric models, and thus this FEM–DS joint approach can save computation time significantly because this method do not involves a particle model consisting of a large macroion and many small bound microions as motioned before (Salonen et al. 2005) but consider a polarized particle as a whole. Therefore, the total number of particles in this DS program could be reduced. It is meanwhile more applicable for complex geometry boundaries and computing domains. The spatial distributions of particles in an energized OET device without an optical pattern are simulated first, and the condition for particle chain formation is discussed. Given that the ring-shaped optical micropattern is the most representative optical pattern used in an OET chip (Chiou et al. 2005; Zhu et al. 2010a, b), which typically reflects and illustrates the main principle of OET phenomena, this study then focuses on the particle dynamics within ring-shaped optical patterns. After the optical pattern is switched on, the influence of the dimensions of optical-ring virtual tweezers on positioning and assembling of particles

is investigated by repeating the dynamics simulation for ring virtual tweezers of different sizes. Additionally, the dynamics simulation model in this study was experimentally verified based on an OET platform, and the experimentally verified results demonstrate that mathematical model describing the microparticles system in an OET device is credible, and the simulation results achieved through FEM and DS joint approach truly reflect the dynamics laws of microparticles in a typical OET device.

2 Model and method

2.1 Structure and physical model of typical OET device

The typical structure of an OET device is shown in Fig. 1a and b, and the simulation work is based on this physical model. The fluidic chamber of this device is set as the computational domain of microparticle dynamics. The photoconductive layer was fabricated by plasma-enhanced chemical vapor deposition (PECVD) and was consecutively deposited with n^+ a -Si:H film with thickness of

50 nm, intrinsic a -Si:H film with thickness of 1.5 μm and SiCx film with thickness of 25 nm on a ITO glass. The equivalent circuit model is shown in Fig. 1c. In this OET device, the conductivity of photoconductive film (a -Si:H) layer in dark environment is approximately $6.7 \times 10^{-5} \text{ S/m}$ and the conductivity of a -Si:H is estimated to increase to 0.2 S/m with strong projected white light source in our platform. The optical pattern can be produced by the DMD-based projector, and then transmitted through several optical reductions and finally projected onto the photoconductive surface of the OET chip controlled by manipulation control software. When an AC voltage signal (its effective voltage is denoted as U_{rms}) is applied to the device and the projected optical pattern with specific shapes is projected to the chip, the photoconductive film is divided into bright and dark areas, the optical bright-dark pattern. The optical pattern projected on the photoconductive layer in the OET device is similar to the metal electrode pattern in the DEP microsystems (Khoshmanesh et al. 2010; Zhu et al. 2010c); hence the optical pattern is also visually called virtual electrode or virtual tweezers. Owing to the conductivity variation across the photoconductive film, there are varying drops in voltage within light and dark areas; thus a specific non-uniform electric field is generated. The voltage drops across the liquid layer within light and dark regions, U_L and U_D , respectively, can be calculated according to the thickness, conductivity, and permittivity of each film layer.

2.2 Mathematical model for multiple forces on particles in OET device

The non-uniform electric field can be generated by selectively illuminating the photoconductive layer inside the OET device, and then the polarized microparticles suspended in the fluidic chamber of the OET device will be driven by DEP force. The expression of the DEP force acting on the i th spherical particle can be approximately expressed in terms of dipole effects as (Chiou et al. 2005; Lin et al. 2006):

$$F_{\text{DEP},i} = 2\pi R^3 \epsilon_m \beta \nabla E_i^2 \tag{1}$$

where R is the radius of particles, ϵ_m is the permittivity of solution, E_i is the electric field intensity (root-mean-square value) at the position of the i th particle, $\beta = \text{Re}[(\epsilon_p^* - \epsilon_m^*) / (\epsilon_p^* + 2\epsilon_m^*)]$ is the real part of Clausius–Mossotti (CM) factor, ϵ_p^* and ϵ_m^* are the complex permittivities of particles and solution, respectively. $\epsilon^* = \epsilon - j\sigma / (2\pi f)$, σ denotes the conductivity and f denotes the frequency of the alternating current (AC) signal.

Besides the dielectrophoretic force, polarized particles are also driven by interacting electrostatic forces between

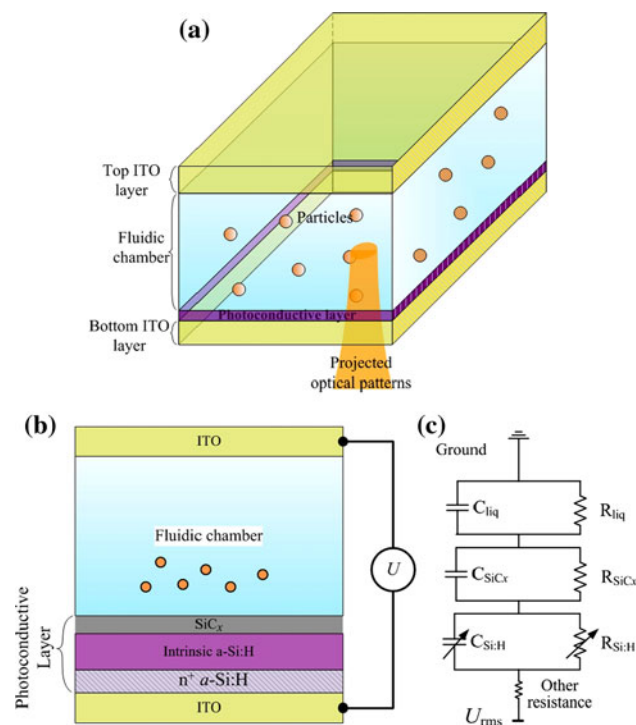


Fig. 1 Structure and equivalent circuit of OET device. **a** Schematic 3D structure of OET device. **b** Cross-section view of the OET device and structure of photoconductive layer. **c** Equivalent circuit of OET device. The capacity and resistance of the a -Si:H layer will change when the light illumination is switched on from off state. Other resistance was measured as about 1.3 Ω totally, including the ITO resistance and the contact resistance existing between the electric wire and ITO layer

particles because the polarization also generates an electric field of its own. For any two polarized particles i and particle j , their electrostatic interacting force $\mathbf{F}_{D,ij}$ can be approximately described as Eq. 2 when the radius is less than electrode's characterized parameter (Kadaksham et al. 2004; Lin et al. 2006):

$$\mathbf{F}_{D,ij} = \frac{3}{4\pi\epsilon_m r_{ij}^5} \left(\mathbf{r}_{ij}(\mathbf{p}_i \cdot \mathbf{p}_j) + (\mathbf{r}_{ij} \cdot \mathbf{p}_i)\mathbf{p}_j + (\mathbf{r}_{ij} \cdot \mathbf{p}_j)\mathbf{p}_i - \frac{5}{r_{ij}^2} r_{ij}(\mathbf{p}_i \cdot \mathbf{r}_{ij})(\mathbf{p}_j \cdot \mathbf{r}_{ij}) \right) \quad (2)$$

where \mathbf{r}_{ij} is the distance vector between the center of particle i and the center of particle j , and $\mathbf{p} = 4\pi\epsilon_m R^3 \beta \mathbf{E}$. Then, $\mathbf{F}_{D,i} = \sum_{j,j \neq i}^N \mathbf{F}_{D,ij}$ is the net electrostatic interacting force acting on the i th particle by the other particles (N is the total number of all particles).

The moving particles in fluid are also resisted by fluidic solution. When the i th particle moves in fluid at speed of \mathbf{v}_i , the fluidic resistance is generally expressed as (Morgan and Green 2003):

$$\mathbf{F}_{\text{drag},i} = -6\pi\mu R \mathbf{v}_i \quad (3)$$

where μ is the dynamic viscosity of the fluid. The motion of a given particle will induce a slight flow field in the solvent, which may be felt by other particles, but this effect is not noticeable in the positioning and assembling of particles in the OET device, and is thus ignored in this study.

In addition, any two particles repel each other in the angstrom to nanometer range. In order to simplify calculation, the short-range interactive force of particles i and j can be described as a continuous expression (Parthasarathy and Klingenberg 1996):

$$\mathbf{F}_{P,ij} = -F_{P0} \exp\left(-\kappa\left(\frac{|\mathbf{r}_{ij}|}{\delta_P} - 1\right)\right) \frac{\mathbf{r}_{ij}}{|\mathbf{r}_{ij}|} \quad (4)$$

where F_{P0} is the magnitude of the electrostatic force when two particles are nearest. κ^{-1} characterizes the range of the force. δ_P is the shortest distance between two particles. Based on Eq. 4, $\mathbf{F}_{P,i} = \sum_{j,j \neq i}^N \mathbf{F}_{P,ij}$ is then the net short-range interacting force acting on the i th particle by the other particles. The repulsive force on the i th particle from the boundary of simulation unit has the similar expression:

$$\mathbf{F}_{W,i} = -F_{W0} \exp\left(-\kappa\left(\frac{|\mathbf{r}_i|}{\delta_W} - 1\right)\right) \frac{\mathbf{r}_i}{|\mathbf{r}_i|} \quad (5)$$

where F_{W0} is the maximum force repelling the boundary by a particle, δ_W is the minimum distance between particle and the boundary, \mathbf{r}_i is the perpendicular distance vector between the i th particle and the boundary.

Micro polystyrene (PS) spherical particles are investigated. The magnitude of the mean displacement due to

Brownian motion for spherical particles is given by $|\Delta d| = \sqrt{k_B T_0 t / 3\pi\mu R}$ (Hughes 2003), where k_B is the Boltzmann constant ($1.3806503 \times 10^{-23} \text{ m}^2 \text{ kg/s}^2/\text{K}^1$), T_0 is the temperature (in Kelvin), and t is the time. $|\Delta d|$ can be approximately calculated as $0.293 \text{ }\mu\text{m}$ for the $5\text{-}\mu\text{m}$ radius particle, and as $0.463 \text{ }\mu\text{m}$ for the $2\text{-}\mu\text{m}$ radius particle when using the following parameter values: $T = 293 \text{ K}$, $\mu = 1.0 \times 10^{-3} \text{ N s/m}^2$ and $t = 1 \text{ s}$. Therefore, the particles with a radius larger than $2 \text{ }\mu\text{m}$ could be controllably positioned and assembled with a relative positional error $< 0.5 \text{ }\mu\text{m}$. At this state, Brownian motion could be negligible because it has little effect on the microparticles' motion in this study. At the same time, $\mathbf{F}_{V,i}$ is the sedimentary force on the i th particle due to the density difference of PS beads and de-ionized water used in this study and its expression is:

$$\mathbf{F}_{V,i} = \frac{4}{3}\pi(\rho_p - \rho_m)R^3 \mathbf{g} \quad (6)$$

where ρ_m and ρ_p are the densities of the aqueous solution and microparticles, respectively, and \mathbf{g} is the gravity acceleration.

According to the above conclusions and Newton's second law, motion equation of the i th particle with the mass m_p in fluid can be described as:

$$m_p \frac{d\mathbf{v}_i}{dt} = \mathbf{F}_{\text{DEP},i} + \mathbf{F}_{D,i} + \mathbf{F}_{\text{drag},i} + \mathbf{F}_{P,i} + \mathbf{F}_{W,i} + \mathbf{F}_{V,i} \quad (7)$$

There is no fluidic flow motion in this study. However, for some special applications, if fluidic flow motion needs to be included into this model, the driving force on the particles by fluid motion should be added to the right-hand side of Eq. 7.

The inertia part can be neglected when the solution's viscosity is close to the water's viscosity (Morgan and Green 2003). Therefore, the final equation is:

$$\mathbf{F}_{\text{DEP},i} + \mathbf{F}_{D,i} + \mathbf{F}_{\text{drag},i} + \mathbf{F}_{P,i} + \mathbf{F}_{W,i} + \mathbf{F}_{V,i} = 0 \quad (8)$$

The dimensionless units of length, time, and electric potential are set as L , T and U , respectively, and they are the characteristic parameters for simulation. Substitute Eqs. 1–6 into Eq. (8) and the final simplified equation is described as:

$$\frac{d\mathbf{x}_i}{dt} = P_{\text{DEP}} \mathbf{F}_{\text{DEP},i} + P_D \mathbf{F}_{D,i} + \mathbf{F}_{P,i} + \mathbf{F}_{W,i} + \mathbf{F}_{V,i} \quad (9)$$

In this equation, \mathbf{x}_i is the displacement vector of the i th particle, which indicates the particle position; t is the time in this dynamic system. $P_{\text{DEP}} = 2\beta R^2 \epsilon_m U^2 T / (3L^4 \mu)$, $P_D = 2\beta R^5 \epsilon_m U^2 T / (L^7 \mu) = 3\beta (R/L)^3 P_{\text{DEP}}$. $\mathbf{F}_{\text{DEP},i}$, $\mathbf{F}_{D,i}$, $\mathbf{F}_{P,i}$, $\mathbf{F}_{W,i}$, $\mathbf{F}_{V,i}$ are the corresponding dimensionless expressions for DEP force, electrostatic interaction force, short-range interaction force between particles, short-range repulsive force between particle and boundary, and sedimentary force for the i th particle.

2.3 Simulation model and parameter settings

In the simulation model of microparticle dynamics in a typical OET device, an AC voltage signal of 20 Vpp at 1 MHz and the de-ionized aqueous solution with a conductivity of $\sim 3 \times 10^{-3}$ S/m are applied. In the optoelectronic tweezer device, AC electroosmosis (ACEO) flow effect (Chiou et al. 2008; Hwang and Park 2009) is usually prominent with frequencies below about 100 kHz. Here, the frequency of 1 MHz is chosen in order to avoid the ACEO flow effect. That is mainly because the ACEO is not beneficial for positioning and assembling microparticles in order to form a stable pattern or structure of particles as well as to quantitatively control the interval between particles simultaneously. The OET device can be operated with or without projecting an optical pattern. When there is no micro-optical projecting pattern projected onto the OET device, the particles have the special dynamics' properties under the action of \mathbf{F}_V , \mathbf{F}_W , \mathbf{F}_D , and \mathbf{F}_P forces without the DEP forces (more details can be found in Sect. 3.1). This case does not need any virtual electrode modeling and the boundary condition is simply: the top surface is ground, the bottom surface is with a potential of U_D , and the other boundaries are electric insulating. In contrast, when an optical pattern is projected onto the OET device bottom, the optical virtual electrode must be modeled and the corresponding boundary conditions should be exerted.

The ring-shaped optical pattern is the most typical and common optical pattern used in the OET chip, which representatively reflects and illustrates the main principle of OET phenomena. For instance, the ring-shaped optical electrode can be utilized for several typical applications of particle capturing, concentrating, and transporting (Chiou et al. 2005; Zhu et al. 2010a, b). Therefore, modeling a ring-shaped virtual electrode can provide valuable and representative references for many applications of OET technology. A ring-shaped optical pattern with inner radius R_e and width d_e was employed (the ring-shaped light pattern is stationary in this paper) in this simulation. The effective voltage of light and dark areas is calculated as $U_L \approx 6.4$ V, $U_D \approx 5.2$ V, respectively, according to the geometry of light pattern and physical equivalent circuit model of the OET device. The sectional view of correspondingly solving domain and boundary conditions is shown in Fig. 2. Given that the boundary of the optical electrode on the light path is not explicit, there is a region of transition between the light and dark areas, which forms a halation ring, and a Gaussian function is applied to the inside and outside of the ring boundary symmetrically, as shown in Fig. 2b. In this case, the Gaussian profile of the electrical potential applied to the inside and outside area of the ring can be expressed as $V_{d_i} = 5.2 + Ae^{-\frac{(r-r_0)^2}{2\sigma^2}}/\sqrt{2\pi}\sigma$

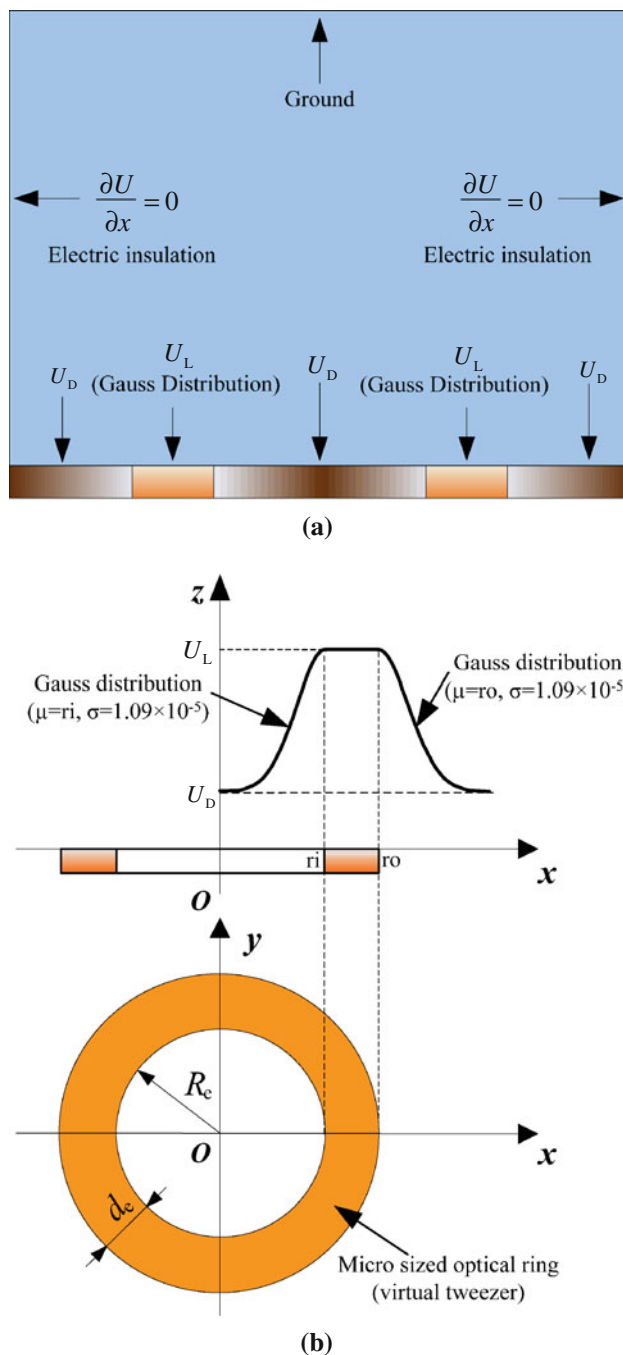


Fig. 2 **a** Sectional view of boundary conditions of the simulation model. **b** Gauss distribution of the electrical potential is applied to the inside and outside of the ring boundary symmetrically. The Gauss distributions on both sides of optical ring characterize the optical projecting system of the OET platform

and $V_{d_o} = 5.2 + Ae^{-\frac{(r-r_0)^2}{2\sigma^2}}/\sqrt{2\pi}\sigma$, where r represents the radial position and A and σ can be calculated as 3.2793×10^{-5} and 1.09×10^{-5} according to the peak value of the Gaussian profile which equals U_L (≈ 6.4 V). Afterwards, the non-uniform electric field in the fluid region of the OET device governed by the Laplace

equation $\partial^2 \varphi / \partial x^2 + \partial^2 \varphi / \partial y^2 + \partial^2 \varphi / \partial z^2 = 0$ (φ is the electric potential) was numerically solved by a commercial finite element program (Comsol Multiphysics 3.2a). After calculating the electric field intensity, electric field gradient, and so forth, in the FEM program, the solved electric field data were then imported into a FORTRAN simulation platform installed in a 64-bit quad-core processor computer.

In the FORTRAN simulation model, the dimensionless units are set as following: $L = 100 \mu\text{m}$, $U = 1 \text{ V}$, and $T = 1,000 \text{ s}$. The simulation domain is a 3D cuboid with bottom side length of $2L$ and height of $0.9L$. The total number of particles is set as N , and the particle's radius is set as $R = 0.05L$ or $R = 0.02L$. The initial heights of the particles are randomized when the optical pattern is switched off, while set as $0.22L$ when modeling the particles' dynamics with the ring virtual electrode projected. The real part of colloid's CM factor β equals -0.474 according to the equation $\beta = \text{Re}[(\epsilon_p^* - \epsilon_m^*) / (\epsilon_p^* + 2\epsilon_m^*)]$ and the input AC signal frequency equals 1 MHz . The DEP force in this study is calculated by using a point-dipole model and without considering the perturbations from the presence of finite-sized particles. And this calculation method for DEP force is applicable here mainly because the particles' initial positions have a height of $0.22L$ above the optical pattern surface and relatively away from the edge of the optical-ring virtual electrode in horizontal direction. In contrast, if the particle is very close to the virtual electrode edge where the length scale of the nonuniformity of electric field is comparable to the particle radius, the distortion of the electric field by the presence of particles should be considered for more accurate calculation (Ai et al. 2009, 2010). Additionally, the expression of CM factor in the point-dipole DEP model is benefit for easily choosing the frequency and solution parameters suitable for the particle assembling within an optical ring.

Finally, simulation time step is set as dt which is in the orders of $10^{-6}T$ to $10^{-7}T$ if there is no special indication (generally, dt needs to satisfy the following condition: $v_{\text{max}} dt < 0.1R$ and v_{max} denotes the maximum velocity of particles) and the total number of simulation steps is set as ts . At the initial moment of simulation, particles are distributed randomly utilizing the "random_seed" function in FORTRAN platform, the initial velocities of all the particles are zero and they are at the same height. Particles' velocities at next moment can be achieved according to Eq. 9 and their displacement coordinates can be achieved by integration of velocities through Velocity-Verlet algorithm (Allen and Tildesley 1989). The particles' coordinates and velocities at different simulation moments can be obtained by continuous cycling computation and the simulation of microparticles' motions under optical virtual

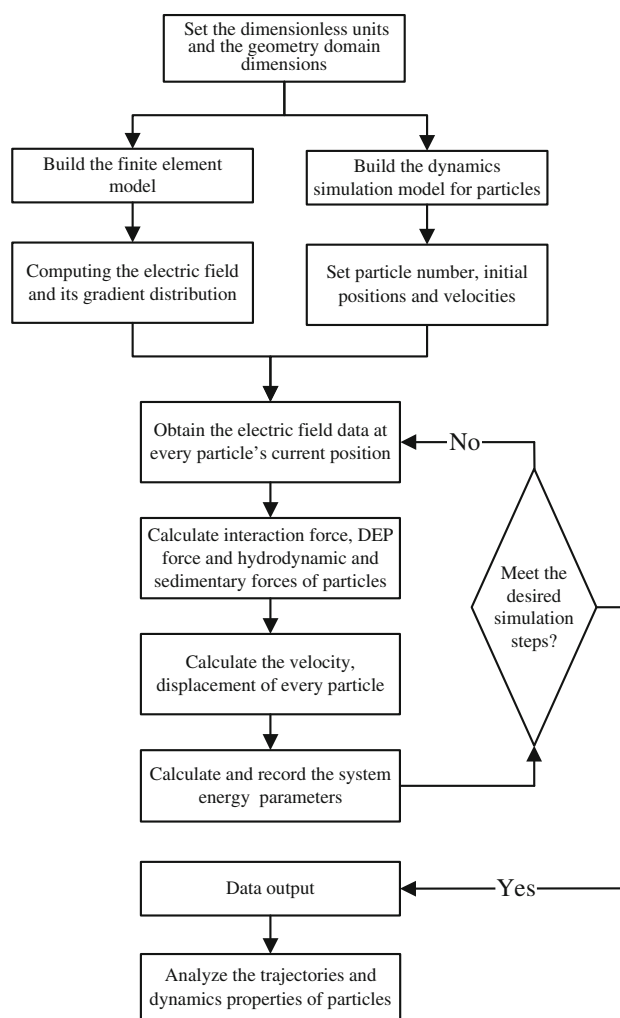


Fig. 3 Flow chart of the dynamics simulation for multiple microparticles in OET device

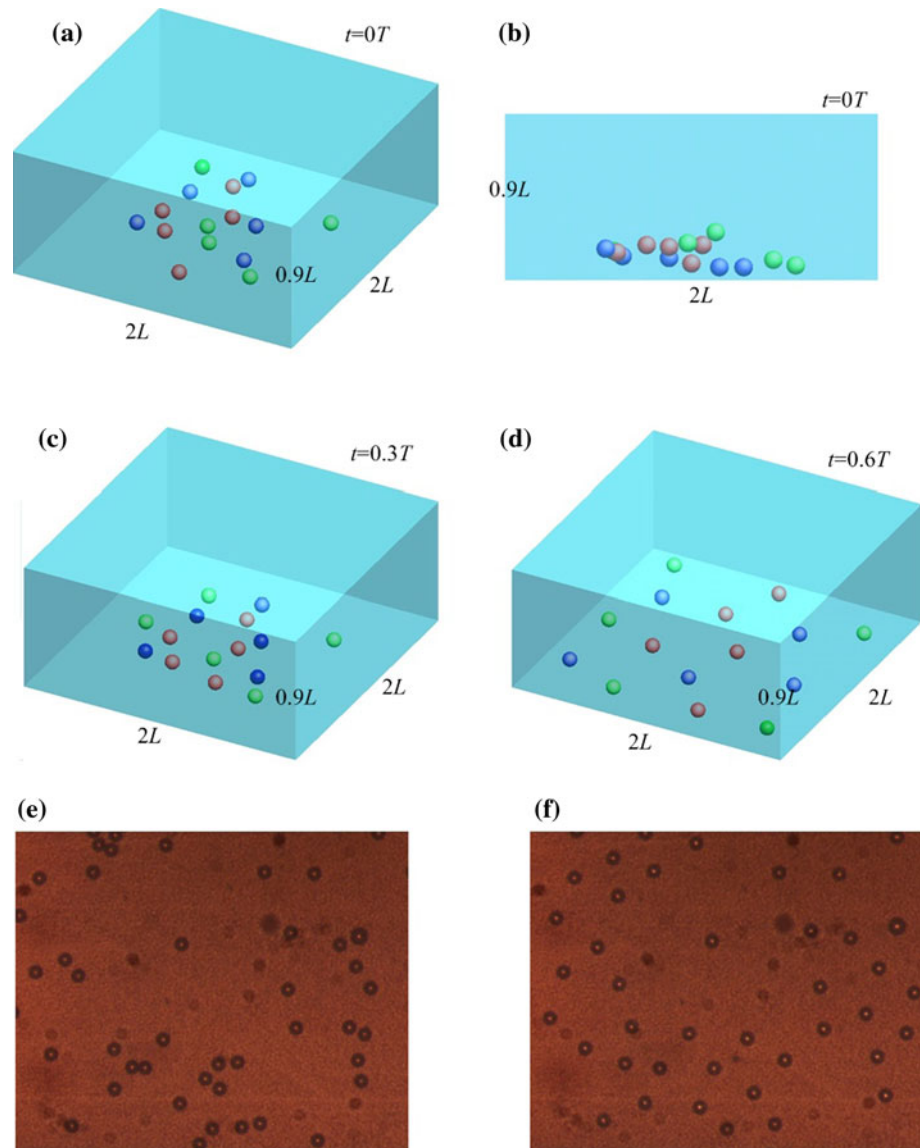
electrode could be completed in this way. The whole flow chart of the dynamics simulation of microparticles in OET device is presented in Fig. 3.

3 Simulation results and discussions with experimental verification

3.1 Particle distribution without optical projecting

The distribution of microcolloids in the electric-signal-actuated OET device without projected light pattern is simulated firstly according to the above simulation settings. The total number of colloidal particles N is 15 and the total number of simulation steps ts is 300,000. At the initial status, all colloidal particles randomly distribute in the 3D fluidic chamber as shown in Fig. 4a and b. The particles are moving freely under the action of \mathbf{F}_V , \mathbf{F}_W and \mathbf{F}_P forces

Fig. 4 **a, b** The 3D view and sectional view of the initial distribution of microparticles with 5- μm radius without input of the AC signal in simulation. **c** The particle distribution at 150,000th step without electrical input and **d** the particle distribution at the 300,000th step after the electrical input was on at the 150,000th step. The experimental distribution of microparticles with 5- μm radius **e** before and **f** after the energization for OET device



without electrical input until all the particles sediment nearly at the bottom of the fluidic chamber at the 150,000th step (see Fig. 4c). At this point the electrical input is suddenly on. Thereafter, the colloidal particles in random distribution disperse gradually and finally are in staggered and uniform distribution upon reaching a equilibrium state (see Fig. 4d), and the distribution destiny decreases from $11.2/L^2$ to $3.8/L^2$. This is because a bias voltage generates vertically across the fluidic chamber and an approximately uniform electric field is thus created in the fluidic chamber. The particles disperse gradually is mainly caused by electrostatic force F_D between the adjacent dipoles of particles induced by the vertical electric field. The whole system is rearranged to a dynamic stable distribution at last. It follows that all the particles are able to be positioned in a relatively incompact form and each particle has a fixed position in OET

device even without projected optical pattern. Moreover, the final distribution destiny of particles could be controlled by the fluidic chamber size and the particle number.

In order to verify the simulation method and results, corresponding experiments are implemented based on the OET platform established by our group (Zhu et al. 2010b). The observation images of microparticles can be acquired by a charge-coupled device camera (Imaging Source Europe GmbH, Germany) connected to the upright microscope (Nikon ECLIPSE 50i) observation port. Solution containing PS beads (Duke Standards, mean diameter $10 \pm 0.05 \mu\text{m}$) with a conductivity of $3 \times 10^{-3} \text{ S/m}$ is chosen for the experiments in this study. The experimental results indicate that PS particles concentrated in stochastic groups before the input of the signal (shown as Fig. 4e). After the input of the signal, approximately stationary

particles moved away from surrounding particles slowly and distributed in a relatively uniform form with nearly equal distance between particles after 1–2 min (shown as Fig. 4f). The experimental phenomenon agrees well with the simulation result.

In the above simulation, the electrical input was switched on after all particles settled on the bottom of fluidic chamber where all particles are in fact at the same height. The following simulation will focus on the case that the particles have not subsided to the chamber bottom when the electrical input is switched on. Initially, the particles distribute randomly at the different heights in the fluidic chamber and the initial positions of particles are also set as presented in Fig. 4a and b for the following simulation. In the simulation, $dt = 2 \times 10^{-4}$ s, $ts = 150,000$. The chain formation of particles in vertical directions at $t = 0.3T$ is presented as shown in Fig. 5a and b. This simulative result of vertical particle–particle attraction is consistent with some published experimental results (Hwang et al. 2008b; Hwang and Park 2011). In the case shown in Fig. 5a, the DEP force can be neglected because of the *uniform* electric field, and the electrostatic interaction force is the dominant force on particles. Referring to Fig. 5c and Eq. 2, the electrostatic force acting on particle-p1 can be calculated as

$$\mathbf{F}_{D,12} = \frac{12\pi\epsilon_m\beta^2R^6E^2}{r_{12}^4}(\mathbf{e}_r + 2(\mathbf{e}_r \cdot \mathbf{z})\mathbf{z} - 5\mathbf{e}_r(\mathbf{z} \cdot \mathbf{e}_r)^2) \quad (10)$$

where \mathbf{z} is the unit vector along the z -axis, \mathbf{e}_r is the unit vector along the vector \mathbf{r}_{12} , and \mathbf{e}_n is the unit vector perpendicular to \mathbf{e}_r as shown in Fig. 5c. Then, Eq. 10 can be rewritten as

$$\mathbf{F}_{D,12} = \frac{12\pi\epsilon_m\beta^2R^6E^2}{r_{12}^4}((1 - 3\sin^2\theta)\mathbf{e}_r - \sin 2\theta\mathbf{e}_n) \quad (11)$$

where θ is the intersection angle between \mathbf{r}_{12} and the horizontal plane. From Eq. 11, electrostatic force \mathbf{F}_D between two particles is perceived as repulsive force when $1 - 3\sin^2\theta > 0$, e.g. $0^\circ \leq \theta \leq 35.3^\circ$, while \mathbf{F}_D is perceived as attractive force when $1 - 3\sin^2\theta < 0$, e.g. $35.3^\circ < \theta \leq 90^\circ$. Consequently, particles could be assembled to form pearl chains in vertical directions when the particles suspended at different heights, and this sort of pearl chain formation can only be obtained when two adjacent particles have the special relative positions as stated above. In the OET device, many particles are usually freely and randomly suspended at different heights without any external control, so the possibility of satisfying the above particle-chain formation conditions is very large as indicated in the simulation results. Additionally, the particle–particle electrostatic force is calculated without considering the perturbations from the presence of finite-sized

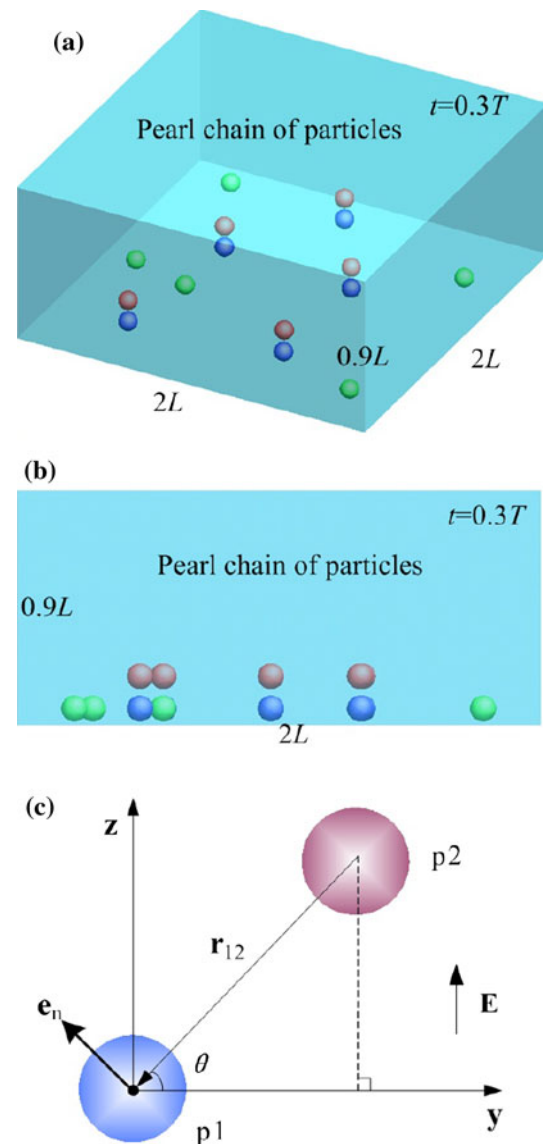


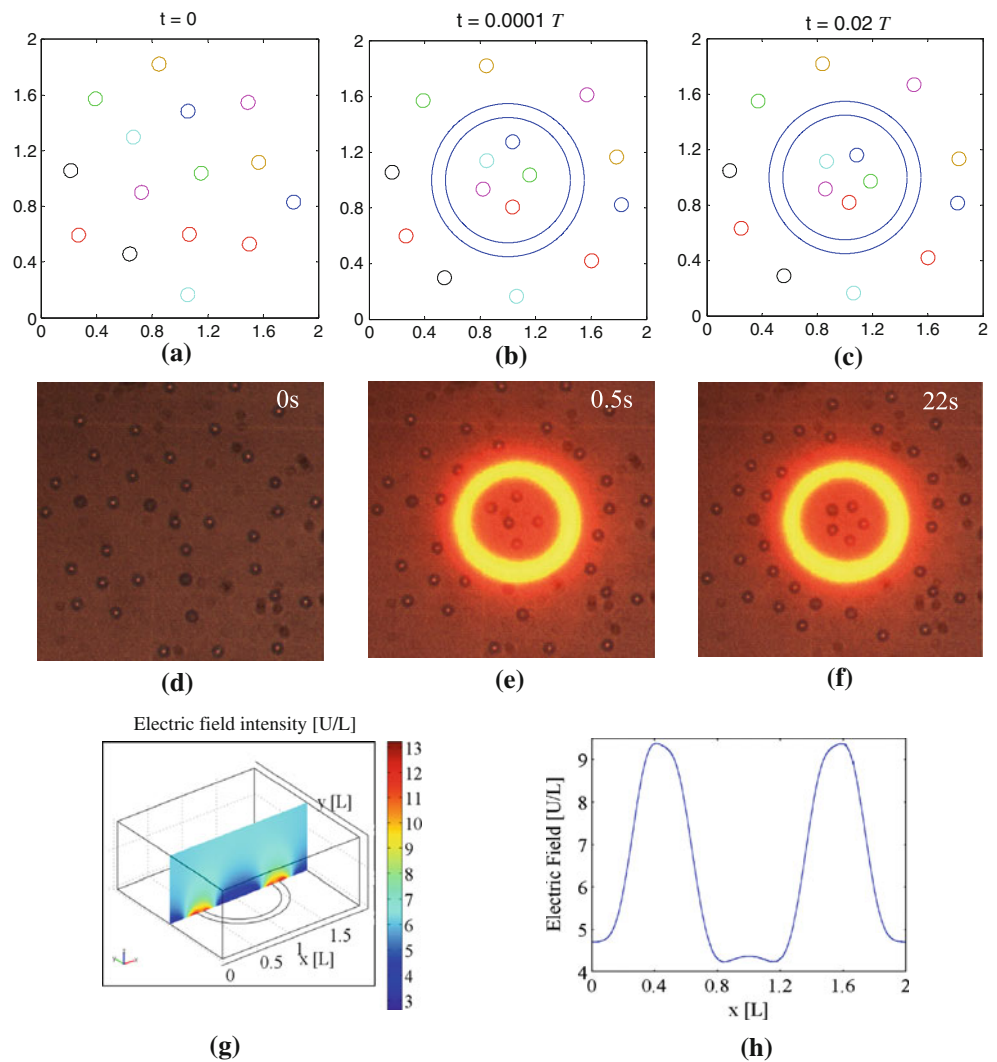
Fig. 5 a, b The simulative formation of particle pearl chain in vertical directions. c The schematic of the electrostatic interaction between two particles

particles. Although this will affect the accuracy of particle–particle electrostatic force, the calculation of electrostatic interacting force $\mathbf{F}_{D,ij}$ based on the effective dipole moment method still has adequate accuracy for predicting the spatial distribution of particles and meanwhile has a high computing efficiency.

3.2 Distribution of particles within optical ring in OET device

After the above simulation for particle distribution without optical projection, the following research work focuses on the particle distribution under the action of the optical-ring virtual electrodes (or called ring virtual tweezer). An

Fig. 6 Simulative and experimental of 5- μm radius particles' trajectories under ring electrode and electric filed analysis. **a–c** The simulation result of the particle distribution varying with time. **d–f** The experimental result of the particle distribution varying with time. **g** Computed distribution of electric field intensity in the middle cross-section (slice at $y = 0$). **h** Profile of electric field intensity at $z = 0.08L$ along the x -direction in the middle cross-section



optical-ring electrode with inner radius $R_e = 50 \mu\text{m}$ and width $d_e = 10 \mu\text{m}$ is employed in the simulation model and the dynamics simulation is then implemented. Particles' positions varying with time calculated from the simulation model after the input of ring virtual electrode are indicated in Fig. 6a–c: the inner particles distribute in the symmetrical and concentrative structure while outer particles distribute in the uniform and disperse structure. In verification experiments, the optical ring produced by the DMD-based projector was projected through several reduction optics onto the photoconductive surface of ODEP chip controlled by manipulation software developed by our group, and the experimental results are shown as Fig 6d–f. The laws of particles' motion and distribution both in experiment and simulation are similar. However, the time instant 0.5 s in Fig. 6e may still a little larger than the $0.0001T (=0.1\text{ s})$ in Fig. 6b when the simulative and experimental particle distributions have the nearly same pattern. This is because there is possibly a little difference

between the actual physical property of the photoconductive layer in OET device and that in the simulation model.

Additionally, the inertia part was neglected in Eq. 7 so that there is a little error between the experimental and simulative motion of particles during the initial acceleration of particles within a very short time.

Particles' distribution results can be explained as following: the real part of the CM factor of the polarized colloidal particle is minus ($\beta < 0$) after the input of AC signal (20 Vpp, 1 MHz). Therefore particles' motion is negative dielectrophoresis, and thus particle will move along the direction which electric field intensity reduces in Fig. 6g shows the 3D numerical simulation of the distribution of electric field under the illumination of a circular optical ring. The profile of electric field intensity at the height of $0.08L$ above the domain bottom surface in the y -direction cross-section in Fig. 6g is shown in Fig. 6h. Electric field intensity decreases sharply from outside to inside along the radius direction inside the electrode and

increases a little near the center of the ring electrode. As a result, the particles inside the ring electrode move from the periphery area to the central area and distribute in an equilibrium structure again under the action of electrostatic force and interactive force. The structure is obviously central symmetric with the geometrical symmetry feature of ring electrode. On the other hand, electric field intensity outside the ring decreases sharply away from the center in radial direction, therefore the outside particles move away from the electrode under negative dielectrophoresis.

3.3 Dynamics of capturing and positioning of particles by optical ring

Flexible and controllable optically induced ring electrode can be employed to capture, position and assembly micron particles within a tiny region under the microscope, which is meaningful in microfluidics applications such as detecting bioparticles of interest or constructing special microstructure with particles. In an OET device, large working range can be achieved just by simultaneously using several or many optical rings (i.e. optical-ring array). Each optical ring is only responsible for the particles within it. The particle dynamics in each optical ring would be the same. Therefore, the most important research work should be focused on the particle dynamics in one optical ring in which the particles can distribute symmetrically and then form special and useful structure automatically through certain kinetic processes. Based on the above simulation model and parameter settings, four particles' capturing processes under virtual ring electrodes with varied geometric parameters are simulated and discussed as follows.

At the initial time, four particles under the actuation of electric voltage were assumed to distribute uniformly with the centers of four particles composing a square with side length of $\sim 30 \mu\text{m}$ at the height of $0.22L$ before the optical ring appears. Then, the microparticles were captured by a ring virtual electrode with dimensions of $R_e = 35 \mu\text{m}$ and $d_e = 10 \mu\text{m}$ in simulation. The simulative trajectories of $5\text{-}\mu\text{m}$ radius particles are shown in Fig. 7a: four particles far away from the ring center are driven by DEP force and start moving toward the center in the direction in which electric field intensity decreasing fastest (that is radius direction) and rebalance under the action of electrostatic force and short-range force finally. The total simulation takes about 15,840 simulation steps from the initial moment to rebalance. Particles' average displacement D (referring to Fig. 7a) is about $11.1 \mu\text{m}$. The variation of horizontal DEP force F_{DEP} , electrostatic force F_{D} and short-range force F_{P} with particles' average displacement are shown as Fig. 7b. With the increment of displacement from the periphery to the center area inside the ring, F_{DEP} decreases from 101.1 to 24.0 pN dramatically, while both

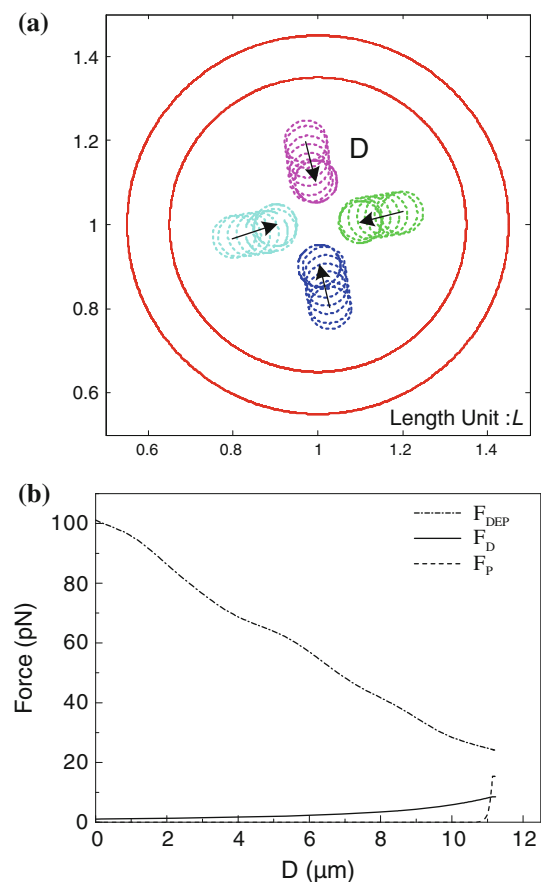


Fig. 7 **a** Motion trajectories of four particles by the action of ring virtual electrode. **b** The dependencies of multiple forces on the particle displacement D

F_{D} and F_{P} increase a little and their maximums are still smaller than F_{DEP} . It can be seen that DEP force is dominant for determining particles' motion in this case, and particles' motion velocity will determine the equilibrium time. Therefore DEP force is the decisive factor influencing the equilibrium time needed for particle positioning and assembling.

3.4 Dynamics of microparticle positioning and assembling using optical rings with different geometry dimensions

The distribution of the non-uniform electric field generated by optical virtual electrode has a remarkable dependence on virtual electrode's geometric dimensions, so the positioning efficiency and assembling effect will change correspondingly. In order to control the positioning and assembly of multi-particles and make every particle occupy specific position, the dynamics simulations for an optical circle-ring with diverse radius and width are implemented. The particles with 5- and $2\text{-}\mu\text{m}$ radius particles (Duke

Standards) were both employed in this study. The aqueous solution containing 2- μm radius PS beads also has a conductivity of 3×10^{-3} S/m.

3.4.1 Influence of optical ring's inner radius on dynamics of particles

In order to analyze the influence of electrode's inner radius on particles' assembling and positioning effect and efficiency, four particles are recaptured in the simulation model and dynamics simulation is implemented again by keeping electrode's width d_e invariable ($d_e = 10 \mu\text{m}$) and changing the inner radius R_e . At each initial state, the geometric centers of particles are stochastically distributed on the same geometric circle with a 20- μm radius for 5- μm particle and a 10- μm radius for 2- μm particle at the same height. The average distances between particle and the center of ring electrode (ADPC) after equilibrium (refer to Fig. 8a) is defined to characterize the particle final positions for different electrodes' inner radii. The simulation result for ADPC is compared with the corresponding verification experiments for both 5- and 2- μm radius particles. As shown in Fig. 8a, both the simulation and experimental values of ADPC increase drastically and monotonically with the increase of R_e , and the simulation result is in qualitative agreement with experimentally observed trend. Therefore, the dynamics simulation model is able to predict the positions of the assembled particles. It follows that we can control the geometric structure of assembled particles and the intervals between particles by subtly tuning the radius of optical ring. Nevertheless, further discussion is needed for interpreting the small differences between simulative and experimental data. As shown in Fig. 8a, the simulative value of ADPC is relatively smaller than the experimental value as R_e decreases below 45 μm for both 5- and 2- μm radius particles. For instance, the relative error is about 22.2% when R_e equals 35 μm for 5- μm radius particle and the particles aggregate more fiercely in simulation. This is probably because the dipole of the particle itself induced by external electric field also causes an electric field with inverse directions, which could in turn counteract and weaken nearby external electric field in practical experiment. This effect exhibits more conspicuously when the R_e decreases below 45 μm for both 5- and 2- μm radius particles is probably because the particles are closer to each other and the closer particle dipoles have more impact on the nearby external field, which leads to smaller DEP forces than the ideal DEP force values in simulation model. As a result, the particles in experiment radially moved inward for a shorter distance (e.g. larger ADPC) than that in simulation. On the other hand, the

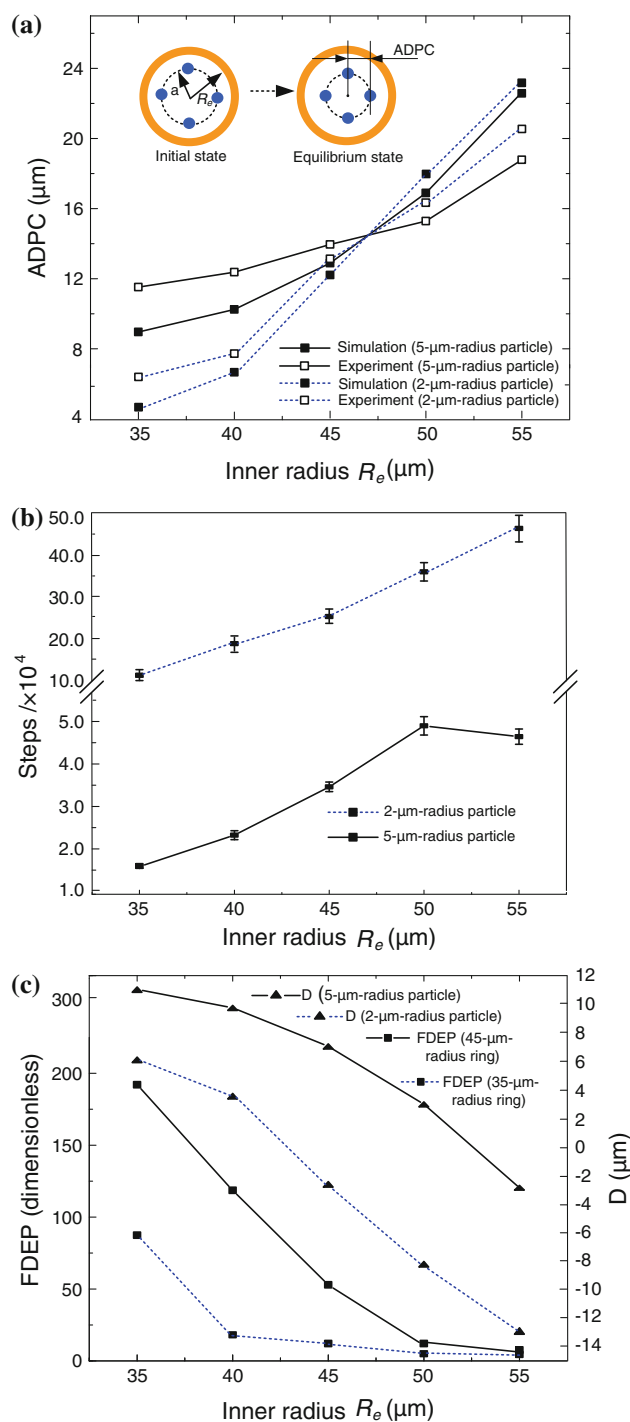


Fig. 8 The dynamics law for assembling particles under different ring virtual electrode's inner radius R_e . **a** The variation of ADPC with R_e . The geometry centers of particles were randomly distributed on the same geometric circle with a radius a (constant value) at initial state for each time calculation. The values of a are 20 μm and 10 μm for the 5- and 2- μm radius particles, respectively. **b** The variation of the equilibrium steps with ring inner radius R_e . **c** The variation of FDEP (mean value) at particle initial positions and the displacement D with ring inner radius R_e

simulative ADPC is higher than the experimental value as the virtual electrode's radius increases above 50 μm . For instance, simulative ADPC value of 5- μm particle is 20.2% higher than the experimental value when R_e equals 55 μm as shown in Fig. 8a. This could be mainly interpreted as follows: the simulative vertical DEP force on particles at the fixed initial positions for the large 55- μm radius ring is weaker than that for the smaller ring, and thus the errors in FEM and MD numerical calculations relatively become conspicuous, which makes the vertical DEP force overestimated. Thus the particles in simulation are levitated to a height higher than actual situation, resulting the exponentially decreasing of horizontal DEP force in simulation. Thus, the simulative repelling force ($\mathbf{F}_D + \mathbf{F}_p$) between particles is stronger over the horizontal DEP force. Consequently, the circular symmetric particles are less aggregated giving rise to higher value of ADPC in simulation.

As shown in Fig. 8b, the influence of electrode's inner radius R_e on particles' assembling and positioning efficiency is presented. In Fig. 8b, the vertical axis represents simulation steps from the initial moment to the new equilibrium; the error bars are sample standard deviation of simulation steps under different radii. In Fig. 8b, the total number of simulation steps increases from 15,800 to 49,000 ($dt = 1 \times 10^{-4}$ s, 10,000 steps equals about 1 s) for the 5- μm radius particle and increases from 111,000 to 373,000 steps for 2- μm radius particle when R_e increases from 35 to 50 μm , and correspondingly the positioning efficiency decreases by about 68 and 70% for the 5- and 2- μm radius particles, respectively. It is noteworthy that the smaller R_e can achieve higher positioning efficiency within the capturing optical ring, which could be much helpful for the high-efficiency assembling and positioning of microparticles. It is also noticeable that the equilibrium time exhibit different variation tendency between the 5- and 2- μm radius particles when R_e increases over 50 μm .

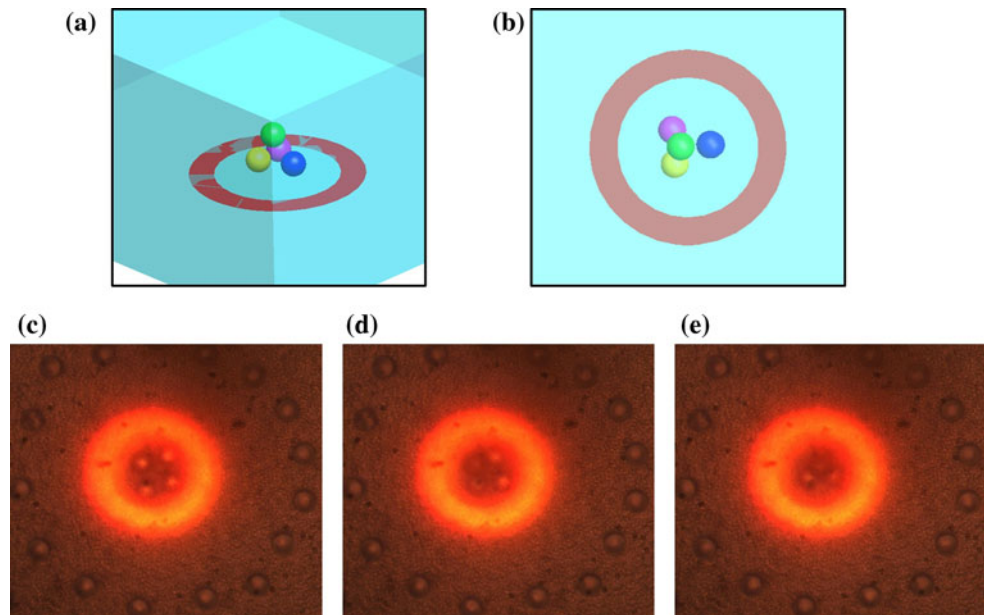
The above phenomenon can be further explained according to particle's horizontal DEP force FDEP and radial displacement D inside the optical ring as shown in Fig. 8c. Dimensionless DEP force (FDEP) decreases from 192 to 11, and the average radial displacement (D) of 5- and 2- μm radius particles decrease from about 11.1 to 2.6 μm and from about 6.0 to -13.1 μm with R_e increasing from 35 to 50 μm . The negative value of D indicates the particles moved away from the ring center and got scattered. The D decreases with the increase of R_e , however, the equilibrium time drastically increases (see Fig. 8b) with R_e below 50 μm , which can be attributed to the sharply drop of FDEP in a near-linear style shown in Fig. 8c, resulting in a sharply decrease of particle radial velocity versus R_e and thus particles need more time to reach equilibriums for larger R_e . Moreover, when virtual electrode's inner radius increases above 50 μm (see Fig. 8c),

the FDEP induced by both two optical-ring sizes at particle initial positions vary only a little but the particles possibly move in opposite direction (the value of D is negative) and get more scattered, so this reverse movement of particles could be attributed to electrostatic repulsive force between particles which is much larger than the DEP force at this time.

There is another noticeable phenomenon when the optical-ring radius R_e decreases below 30 μm for the 5- μm radius particle. The 3D simulation results of the forces acting on particles within optical ring also indicate that the horizontal repulsive force and vertical attractive force between adjacent particles both increase sharply with the shrinking of optical ring in radius direction when the virtual R_e is smaller than 30 μm but larger than 13 μm . In this situation, particles do not distribute at the same height but distribute in split-level structure as shown in Fig. 9a and b. Similar phenomena observed in the verification experiment are shown in Fig. 9c–e. Four PS beads initially distributed in central symmetry structure when R_e decreased to 25 μm (shown in Fig. 9c), but this structure was not stable. The particles driven by DEP force went on moving to the ring center as shown in Fig. 9d and were then repelled by each other until the limit intervals between particles were reached. Because of particles' asymmetrical distribution due to subtle differences in electro-properties of particles, the particle closest to the optical-ring center experienced the largest repulsive force and this particle then started moving along vertical direction and quickly jumped above the other three particles within about 1–1.5 s. The final equilibrium distribution is shown in Fig. 9e, the original particle staying close to the ring edge finally levitated above the other particles and the other particles still distributed in approximately central symmetry structure on the bottom, which forms a micropyramid consisting of four particles. This kind of particle spatial distribution may bring new approach to assembly particles forming specific 3D microstructures.

The above analysis indicates that DEP force decreases, system equilibrium time increases, and a larger ADPC value could be achieved with the increment of ring radius. Moreover, particles will pile up to form 3D micropyramid structure when the optical-ring radius decreases to a threshold value. Besides, virtual optical electrodes of large radius usually occupy large operating space correspondingly and the positioning accuracy may become low. Consequently, to achieve higher capturing and positioning efficiency and larger positive displacement D , the ring electrode's inner radius is suggested to be set as 35–45 μm when positioning and assembling four 5- or 2- μm radius PS beads if there is not special application requirement. To construct 3D structure of particles, the ring inner radius should be gradually reduced until a particle starts to jump

Fig. 9 Simulative and experimental results for particle assembly in 3D space by a shrinking optical-ring virtual electrode. **a** The microparticle pyramid structure consisting of four 5- μm radius particle according to the simulative results. This plot is created exactly according to the computed coordinates of every particle from the simulation program. **b** Top view of the microparticle pyramid structure. **c–e** Snapshots of the experimentally assembling of the microparticle pyramid consisting of four 5- μm radius particle



up above other particles. As a corollary of this research work, parallel assembling microparticle structure including the 3D microparticle pyramid shown in Fig. 9 in array form could be also achieved by using a massively array of optical-ring virtual tweezers.

3.4.2 Influence of optical ring's width on dynamics of particles

In addition to the radius R_e , the width of the optical-ring electrode d_e is also a contributing physical quantity for controlling the particle assembling and positioning. According to the simulation results, electric field intensity and gradient around the virtual electrode vary with the width of ring electrode d_e . Therefore, the capturing and positioning effect varies correspondingly. In simulation, the initial positions of particle centers are randomly distributed in on the same geometric circle with a 20- μm radius for 5- μm particle and a 10- μm radius for 2- μm particle at the same height, and the virtual electrode's inner radius keeps invariable ($R_e = 45 \mu\text{m}$ for 5- μm radius particle and $R_e = 35 \mu\text{m}$ for the 2- μm radius particle), and the particles' dynamics under different optical-ring widths is computed based on the FEM–DS simulation model and the effect on particles' positioning efficiency is analyzed. Figure 10a shows the simulative and experimental values of ADPC versus the ring width d_e . ADPC decreases slightly with the increment of d_e nevertheless the total variation is $<1.2 \mu\text{m}$ for the 5- μm radius particle and $0.8 \mu\text{m}$ for the 2- μm radius particle. Each ADPC curve approximately tends to a constant after d_e increases to 20 μm . Therefore, ADPC varies slightly with the increase of d_e , which means the ring electrode's width has very little

impact on positioning and assembling control. Simulation result agrees well with the experiment result as shown in Fig. 10a and the maximum relative error is $<5.0\%$.

The variation of positioning efficiency with ring electrode width d_e could be indicated by the number of computing steps ($dt = 1 \times 10^{-4} \text{ s}$) varying with d_e in simulation which is shown in Fig. 10b, and the error bars represent sample standard deviation of simulation steps. When d_e equals 10 μm , the total number of equilibrium steps for both 5- and 2- μm radius particles have a minimum value, and at this moment the positioning efficiency is highest. The system equilibrium time increases apparently with the increase of d_e ranging from 10 to 20 μm . When d_e is larger than 20 μm , the equilibrium time fluctuates around $0.0045T$ (45,000 steps) approximately for 5- μm radius particle but has a noteworthy decrease for 2- μm radius particle. The ring width of 10–15 μm will be modest to achieve relatively high positioning efficiency although the ring with width of 10–15 μm is unhelpful to achieve small ADPC values for assembled particle, but this drawback can be overcome by adjusting the inner radius R_e referring to Fig. 8a.

As shown in Fig. 10c, with the increment of d_e , the variation in radial displacement D is very small (the varied range of D is $<0.5 \mu\text{m}$ for both two kinds of particle radii) and the horizontal DEP force F_{DEP} also varies very slightly, compared with the variation of D and F_{DEP} with respect to R_e (referring to Fig. 8c). The 5- and 2- μm radius particles were trapped by a ring with 45- μm inner radius and a smaller ring with 35- μm inner radius, respectively. The F_{DEP} for 2- μm radius particle is always larger than that for 5- μm radius particle is mainly because the smaller radius of light ring causes a more sharp variation of the

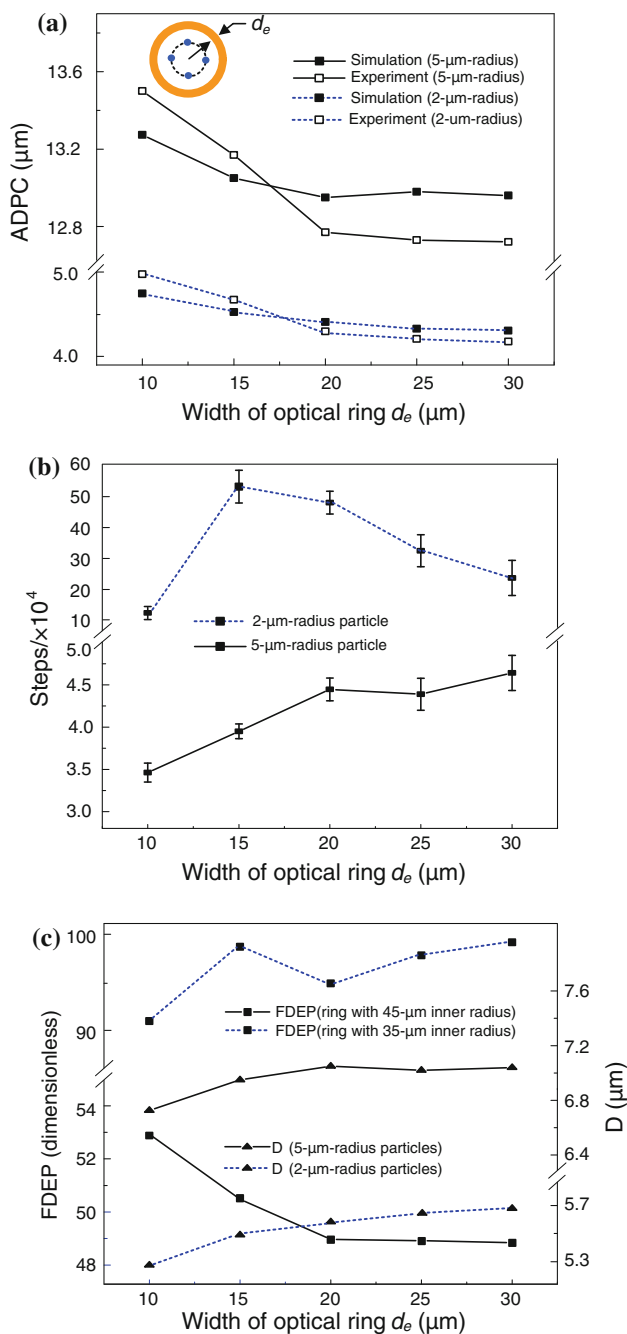


Fig. 10 The dynamics law for assembling particles under different ring virtual electrode's width d_e . **a** The dependence of ADPC on d_e . The values of R_e are set as $R_e = 45 \mu\text{m}$ for 5- μm radius particle and $R_e = 35 \mu\text{m}$ for the 2- μm radius particle. **b** The variation of equilibrium steps number with d_e . **c** The variation of FDEP (mean value) at fixed initial positions inside the optical ring and the radial displacement D with the width of optical ring d_e

electrical field inside the ring resulting in larger field gradients. The variations of FDEP versus d_e for both two sorts of ring radii (35 and 45 μm) are both very slight and are < 9 which are significantly much smaller than the range of FDEP variation caused by changing R_e of the optical ring

as shown in Fig. 8c. Within the optical ring of 45- μm inner radius, the horizontal DEP force at particle initial positions inside the ring decreases slightly with the increase of d_e but vary only a little when d_e is larger than 20 μm . Within the optical ring of 35- μm inner radius, the fluctuation of the FDEP on the 2- μm radius particle is more conspicuous than that in the 45- μm radius ring, but also in a small variation range, which is possibly caused by numerical errors in the FEM calculation of electric field and data import process. When d_e is larger than 25 μm , both FDEP and radial displacement D are not sensitive with the change of d_e , which is possibly because the electric field distribution is nearly independent on the width of the optical ring when the inside radius of ring is relatively large.

The sensitivities of positioning and assembling effect and efficiency to ring electrode's inner radius and width are distinctly different according to the comparison between Figs. 8 and 10. The available varying range of ADPC by tuning R_e is apparently larger than that by tuning d_e through comparing Figs. 8a and 10a. For instance, If an ADPC value smaller than 12.5 μm for 5- μm radius particle needs to be obtained, the reasonable choice is to tuning R_e because the minimum ADPC value can be achieved by tuning d_e is still larger than 12.5 μm . On the other hand, the system equilibrium time of the 5- μm radius particle increases approximately 2.1 times when R_e increases from 35 to 55 μm (the increment is 20 μm), while the system equilibrium time increases approximately only 0.3 times when d_e increases from 10 to 30 μm (the increment is also 20 μm). That means the average increase rate of equilibrium time versus R_e is much larger than that versus d_e . Therefore, it could be a more reasonable choice to decrease R_e to get a higher efficiency for 5- μm radius particle. However, for the 2- μm radius particle, there should be a comprehensive consideration of both R_e and d_e to get high assembling efficiency according to the calculated equilibrium time curves shown in Figs. 8b and 10b.

In addition, the radius and width of optical ring can also be both finely tuned to improve the capturing efficiency and positioning accuracy. For instance, if the radius R_e is not allowed to decrease in some special practical applications, the width d_e can be increased for achieving a bit smaller ADPC value. So tuning the radius and width of optical ring can also act as two complementary means to meet specific needs of assembling and positioning micro-particles within a microscale area.

4 Conclusion

A dynamics simulation model coupling DEP force, interaction forces, hydrodynamic and sedimentary forces acting on colloidal particles in optoelectronic tweezer (OET)

device is built in this study. ODEP positioning and assembling of microparticles is simulated through the FEM–DS joint numerical approach. The spatial distributions of particles in energized OET device without optically projected pattern are simulated first and the particles possibly be assembled to vertical chains under the vertical uniform electric field when particles freely and randomly suspend at different heights before they sediment on chamber bottom. Then the dynamics for particles ($R = 5$ and $2 \mu\text{m}$) capturing and positioning driven by optical pattern is simulated. The simulation results indicate that polarized colloids in non-uniform electric field repel each other on the horizontal plane, and particles all move in the negative direction of electric field gradient. The inner particles move towards the optical-ring center, and the outer particles move away from the center, and finally form a circle uniform distribution with the nearly same interval between particles around the circle. The simulation results agree well with the experimental observations.

Moreover, the influences of the dimensions of optical-ring virtual tweezer on positioning and assembling of particles ($R = 5$ and $2 \mu\text{m}$) are investigated by repeating the dynamics simulation for ring virtual electrodes with different dimensions. The simulation results indicate that the value of ADPC increases by about 13.7 and 18.0 μm , and the system equilibrium time increases by about 3.06 and 34.9 s for 5- and 2- μm radius particles, respectively, when R_c is tuned from 35 to 55 μm (d_c equals 10 μm). It is noteworthy that the captured particles possibly pile up to form 3D micropyramid structure or move out of the ring when the radius of ring electrode is gradually reduced until a particle starts to jump up above other particles. Moreover, ADPC decreases only a little and the system equilibrium time increases by ~ 1.18 s for 5- μm radius particle when d_c is tuned from 10 to 30 μm (R_c equals 45 μm), and the equilibrium time nearly remains invariant after d_c reaching 20 μm . However, the system equilibrium time for 2- μm radius particle is several to more than ten times as long as that for 5- μm radius particle, and rises distinctly as d_c is $< 15 \mu\text{m}$ but declines as d_c is larger than 15 μm . The available varying range of ADPC by adjusting R_c is apparently larger than that by adjusting d_c . Additionally, adjusting the width of the optical ring could act as a complementary mean for accurately positioning and assembling microparticles and tuning intervals between particles within a microscale area. The mainly simulation results are experimentally verified and in general the simulation results agree well with experimental data. Therefore, the dynamics modeling approach in this study can predict dynamics laws of positioning and assembling microparticles utilizing the OET device. Moreover, this dynamics simulation model and computing method could provide a powerful simulation platform for designing,

analyzing and optimizing the optical micropatterns and physical structure of OET device.

Acknowledgments This work was supported by National 973 Program of China (2011CB707600), Major Program of the National Natural Science Foundation of China (91023024), New Century Elitist Program by Ministry of Education of China (NCET-07-0180), the Ph.D graduate Academic Award by Ministry of Education of China, and Jiangsu Graduate Innovative Research Program (CX10B_062Z). The authors also thank Di Jiang's assistance during the implementation of partial computation.

References

- Ai Y, Joo SW, Jiang YT, Xuan XC, Qian SZ (2009) Transient electrophoretic motion of a charged particle through a converging-diverging microchannel: effect of direct current-dielectrophoretic force. *Electrophoresis* 30(14):2499–2506
- Ai Y, Park S, Zhu J, Xuan X, Beskok A, Qian S (2010) DC electrokinetic particle transport in an L-shaped microchannel. *Langmuir* 26(4):2937–2944
- Aldaeus F, Lin Y, Roeraade J, Amberg G (2005) Superpositioned dielectrophoresis for enhanced trapping efficiency. *Electrophoresis* 26(22):4252–4259
- Allen MP, Tildesley DJ (1989) *Computer simulation of liquids*. Oxford University Press, Oxford
- Cheng IF, Chang HC, Hou D, Chang HC (2007) An integrated dielectrophoretic chip for continuous bioparticle filtering, focusing, sorting, trapping, and detecting. *Biomicrofluidics* 1(2): 021503
- Chiou PY, Ohta AT, Wu MC (2005) Massively parallel manipulation of single cells and microparticles using optical images. *Nature* 436(7049):370–372
- Chiou PY, Ohta AT, Jamshidi A, Hsu HY, Wu MC (2008) Light-actuated ac electroosmosis for nanoparticle manipulation. *J Microelectromech Syst* 17(3):525–531
- Green NG, Morgan H (1997) Dielectrophoretic separation of nanoparticles. *J Phys D Appl Phys* 30(11):L41–L44
- Hughes MP (2003) *Nanoelectromechanics in engineering and biology*. CRC Press, Boca Raton
- Hwang H, Park JK (2009) Rapid and selective concentration of microparticles in an optoelectrofluidic platform. *Lab Chip* 9(2):199–206
- Hwang H, Park JK (2011) Optoelectrofluidic platforms for chemistry and biology. *Lab Chip* 11(1):33–47
- Hwang H, Choi YJ, Choi W, Kim SH, Jang J, Park JK (2008a) Interactive manipulation of blood cells using a lens-integrated liquid crystal display based optoelectronic tweezers system. *Electrophoresis* 29(6):1203–1212
- Hwang H, Kim JJ, Park JK (2008b) Experimental investigation of electrostatic particle-particle interactions in optoelectronic tweezers. *J Phys Chem B* 112(32):9903–9908
- Jamshidi A (2009) *Optoelectronic Manipulation, assembly, and patterning of nanoparticles*. University of California at Berkeley
- Jamshidi A, Pauzuskie PJ, Schuck PJ, Ohta AT, Chiou PY, Chou J, Yang PD, Wu MC (2008) Dynamic manipulation and separation of individual semiconducting and metallic nanowires. *Nat Photonics* 2(2):85–89
- Kadaksham J, Singh P, Aubry N (2004) Dynamics of electrorheological suspensions subjected to spatially nonuniform electric fields. *J Fluid Eng* 126(2):170–179
- Khoshmanesh K, Zhang C, Tovar-Lopez FJ, Nahavandi S, Baratchi S, Mitchell A, Kalantar-Zadeh K (2010) Dielectrophoretic-

- activated cell sorter based on curved microelectrodes. *Microfluid Nanofluidics* 9(2–3):411–426
- Lee M-W, Lin Y-H, Lee G-B (2010) Manipulation and patterning of carbon nanotubes utilizing optically induced dielectrophoretic forces. *Microfluid Nanofluidics* 8(5):609–617
- Li M, Qu Y, Dong Z, Li WJ, Wang Y (2008) Design and simulation of electrodes for 3D dielectrophoretic trapping. In: 3rd IEEE international conference on nano/micro engineered and molecular systems, 2008. NEMS 2008, 6–9 Jan 2008, pp 733–737
- Lin YH, Lee GB (2008) Optically induced flow cytometry for continuous microparticle counting and sorting. *Biosens Bioelectron* 24(4):572–578
- Lin Y, Amberg G, Aldaeus F, Roeraade J (2006) Simulation of dielectrophoretic motion of microparticles using a molecular dynamics approach. *ASME Conf Proc* 2006(47608):1–10
- Lin WY, Lin YH, Lee GB (2010) Separation of micro-particles utilizing spatial difference of optically induced dielectrophoretic forces. *Microfluid Nanofluidics* 8(2):217–229
- Morgan H, Green NG (2003) AC electrokinetics: colloids and nanoparticles. *Microtechnologies and microsystems series*, 2. Research Studies Press, Philadelphia
- Morgan H, Holmes D, Green NG (2003) 3D focusing of nanoparticles in microfluidic channels. *IEE Proc Nanobiotechnol* 150(2):76–81
- Ni Z, Zhang X, Yi H (2009) Separation of nanocolloids driven by dielectrophoresis: a molecular dynamics simulation. *Sci China Seri E Technol Sci* 52(7):1874–1881
- Ohta AT (2008) Optofluidic devices for cell, microparticle, and nanoparticle manipulation. University of California at Berkeley
- Parthasarathy M, Klingenberg DJ (1996) Electrorheology: mechanisms and models. *Mater Sci Eng R Rep* 17:57–103
- Pohl H (1978) Dielectrophoresis. Cambridge University Press, New York
- Salonen E, Terama E, Vattulainen I, Karttunen M (2005) Dielectrophoresis of nanocolloids: a molecular dynamics study. *Eur Phys J E Soft Matter Biol Phys* 18(2):133–142
- Valley JK, Jamshidi A, Ohta AT, Hsu HY, Wu MC (2008) Operational regimes and physics present in optoelectronic tweezers. *J Microelectromech Syst* 17(2):342–350
- Valley JK, Neale S, Hsu HY, Ohta AT, Jamshidi A, Wu MC (2009) Parallel single-cell light-induced electroporation and dielectrophoretic manipulation. *Lab Chip* 9(12):1714–1720
- Zhu X, Yi H, Ni Z (2010a) Frequency-dependent behaviors of individual microscopic particles in an optically induced dielectrophoresis device. *Biomicrofluidics* 4(1):013202
- Zhu X, Yin Z, Gao Z, Ni Z (2010b) Experimental study on filtering, transporting, concentrating and focusing of microparticles based on optically induced dielectrophoresis. *Sci China Technol Sci* 53(9):2388–2396
- Zhu XL, Gao ZQ, Yin ZF, Ni ZH (2010c) Electrode-rail dielectrophoretic assembly effect: formation of single curvilinear particle-chains on spiral microelectrodes. *Microfluid Nanofluidics* 9(4–5):981–988